

High-quality, high-information datasets for universal atomistic machine learning

Cesare Malosso,¹ Filippo Bigi,¹ Paolo Pegolo,¹ Joseph W. Abbott,¹
Philip Loche,¹ Mariana Rossi,^{2,3} Michele Ceriotti,^{1,*} and Arslan Mazitov¹

¹*Laboratory of Computational Science and Modeling, Institut des Matériaux,
École Polytechnique Fédérale de Lausanne, 1015 Lausanne, Switzerland*

²*MPI for the Structure and Dynamics of Matter, 22761 Hamburg, Germany*

³*Yusuf Hamied Department of Chemistry, University of Cambridge, CB2 1EW Cambridge, UK*

(Dated: March 3, 2026)

The quality, consistency, and information content of training data is often what determines the practical value of machine-learning models for atomistic simulations. Yet, many widely used electronic-structure databases are assembled having materials screening as primary goal rather than robust force-field learning, are limited in their scope to a specific class of chemical compounds, and/or employ inconsistent DFT functionals and settings. Here we introduce MAD-1.5, a highly curated dataset designed explicitly for training broadly applicable atomistic models across the periodic table at high levels of theory. MAD-1.5 extends the MAD dataset with targeted enrichment strategies that improve the coverage of chemical space to 102 elements while keeping the total number of configurations compact. All structures are computed with a single, standardized all-electron DFT workflow using the r²SCAN meta-GGA functional and consistent convergence settings, ensuring uniformity across chemically heterogeneous systems. The dataset encompasses molecules, clusters, bulk crystals, surfaces, and low-dimensional structures, and its quality and consistency are further enhanced by outlier removal using uncertainty quantification. We demonstrate the high accuracy that can be achieved with the proposed dataset by training PET-MAD-1.5, a generally applicable r²SCAN interatomic potential that covers 102 elements in the periodic table and achieves exceptional levels of benchmark accuracy and stability in challenging simulation protocols.

I. INTRODUCTION

Atomistic simulations increasingly rely on machine-learned surrogate models to bridge the gap between first-principles accuracy and the length- and time-scales needed for effective modeling [1–3]. While modern architectures can represent complex potential-energy surfaces, their reliability in practice is often limited by the training data. The coverage of chemical space, the diversity of local environments, and the presence of challenging off-equilibrium configurations in a dataset can determine accuracy in molecular dynamics, structure optimization, and in the description of rare events, of reactions and of interfacial processes [4, 5].

Training broadly transferable interatomic models raises two recurring data challenges. First, many available reference collections are dominated by near-equilibrium structures, which result in models that are not sufficiently constrained in the distorted, high-force, and close-contact regimes that control stability in challenging modeling scenarios, especially at high temperatures. Second, datasets assembled over long periods or from multiple sources often mix electronic-structure settings in subtle ways (e.g., numerical thresholds, treatment of magnetism, or other minor protocol choices), resulting in small, but at times significant, inconsistencies.

Recent learning-oriented datasets address these limitations by explicitly targeting both coverage and con-

sistency [6–10]. However, they fail in achieving a fully universal character in different ways, either because they are limited to a class of chemical compounds (e.g., only extended systems or only molecules), or because they employ electronic-structure settings that are inconsistent between different classes of compounds. Furthermore, large datasets can often contain redundant atomic environments, diluting their information content.

In Ref. 5 some of us introduced MAD, a dataset based on the principle of Massive Atomic Diversity – incorporating different classes of highly-distorted structures, and using consistent and convergent electronic-structure settings, based on density-functional theory (DFT) at the PBEsol [11] exchange-correlation level. To further build on these ideas, we now introduce MAD-1.5, an extension of MAD (from now on referred to as MAD-1) designed to increase chemical completeness and interaction coverage while retaining compactness and reference consistency. All configurations are computed with a single standardized all-electron DFT workflow using the r²SCAN meta-GGA functional [12, 13], which has shown excellent transferability among different chemistries [14–16]. MAD-1.5 expands element coverage up to 102 elements, including every isotope with a half-life above a day, and enriches under-represented portions of chemical space through targeted additions. We characterize the resulting dataset and demonstrate its utility by training a general-purpose machine-learned interatomic potential, PET-MAD-1.5, observing exquisite robustness and transferability across diverse materials and molecular environments.

* michele.ceriotti@epfl.ch

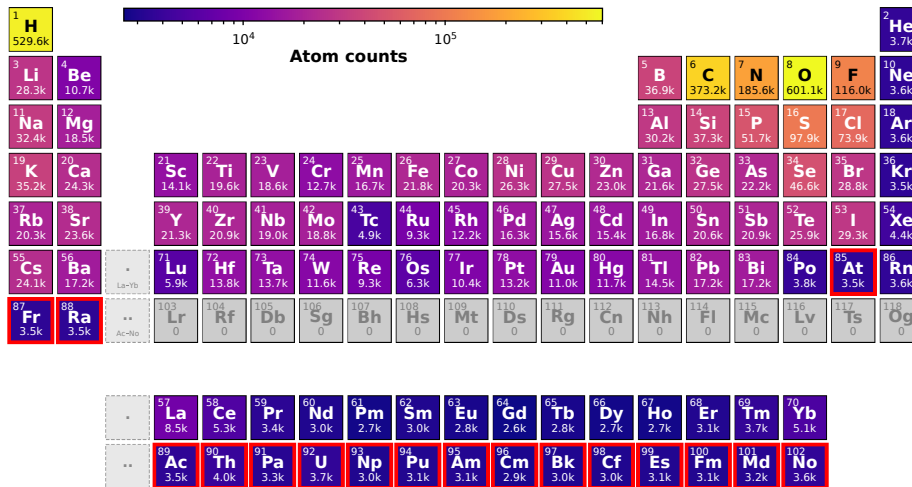


FIG. 1. Periodic table indicating the statistical representation of the elements present in the MAD-1.5 dataset. Each element tile contains the proton number, element symbol, and elemental frequency in MAD-1.5, by which it is also colored. Elements in gray are not present in the dataset, and those bordered in red have been newly introduced to MAD-1.5 compared the original MAD-1 dataset.

II. DATASET CONSTRUCTION

A. Composition

The MAD-1.5 dataset contains 216803 atomic structures spanning 102 chemical elements. It is constructed as an extension of the MAD-1 dataset, augmented with additional structures specifically designed to enrich the coverage and predictive accuracy across the entire periodic table. The element counts of the MAD-1.5 dataset are shown in Fig. 1. The dataset is organized into 14 subsets (summarized in Table I) that span a wide range of chemical compositions and structural motifs, including molecules, clusters, bulk crystals, low-dimensional materials, and surfaces. The structures inherited from MAD-1 (8 subsets) provide a broad baseline of chemically and structurally diverse configurations, including 85 elements, while the newly introduced structures (6 new subsets) systematically target under-represented elements, coordination environments, and bonding regimes. We briefly describe the individual subsets comprising MAD-1.5, outlining their makeup, and how they contribute to extend chemical and configurational coverage.

For a comprehensive description of the structures inherited from MAD-1, we refer the reader to the original publication [5]. Beyond explicit inclusion of *monomers*, new structures introduced in MAD-1.5 span five distinct subsets, each designed to sample different coordination environments and bonding regimes. Analogous to the original *Materials Cloud 3D Database* (MC3D) [17] dataset, the *MC3D-extended* subset contains 11562 periodic structures, but including a broader variety of elements, covering previously missing lanthanides and actinides, as well as additional under-represented main-

group and transition metals. The *MC3D-random-extended* subset addresses the limited representation of heavy elements in MAD-1. It applies the same randomization strategy as *MC3D-random* [5], but with the added constraint that each structure includes at least one of the previously missing or under-represented elements. This approach ensures that the interactions involving these elements are adequately sampled while keeping the total number of configurations minimal and the diversity maximal. The *binary-random* subset contains binary substitutional orderings generated by decorating supercells of BCC and FCC parent lattices with all pairs of chemical species drawn from the 102 elements. We restrict sampling to supercells containing up to three parent-lattice sites and, for each supercell, enumerate all distinct site-occupation patterns compatible with a binary system [18, 19]. Including this set ensures broad chemical coverage and provides a strong prior on interactions across the full set of elements (including chemically atypical pairings) while avoiding the combinatorial growth associated with larger cells and more complex orderings. Cell volumes are chosen such that the average volume per atom is equal to the average van der Waals volume of the elements in the system.

The *dimers* subset explicitly samples two-body interactions across the entire periodic table by systematically generating all unique pairs of 102 elements. For each element pair, interatomic distances are sampled along ten linearly spaced points between a minimum distance of 0.125 times the sum of the van der Waals radii and a maximum distance equal to the sum of the van der Waals radii. This sampling scheme captures the repulsive regime at short ranges, the equilibrium bonding region, and the onset of the long-range tail, providing comprehensive potential-energy curves for all possible ele-

	Subset name	Description	# structures	# atoms
MAD-1 dataset	MC3D	Bulk crystals from the Materials Cloud 3D (MC3D) database	33 343	728 155
	MC3D-rattled	Rattled configurations derived from MC3D	29 214	569 254
	MC3D-random	Atomic species randomized over 85 elements in MC3D structures	2 075	17 052
	MC3D-surface	Surface slabs generated from MC3D crystals	4 928	181 674
	MC3D-cluster	Nanoclusters cut from MC3D and MC3D-rattled structures	8 651	42 867
	MC2D	Two-dimensional crystals from the Materials Cloud 2D database	2 502	40 950
	SHIFTML-molcryst	Curated molecular crystals from the SHIFTML dataset	8 572	851 596
	SHIFTML-molfrags	Neutral molecular fragments from SHIFTML	3 242	72 130
New structures	monomers	Isolated single-atoms covering all 102 elements	102	102
	dimers	Isolated two-atom configurations sampled from 102 elements	31 325	62 650
	trimers	Isolated three-atom configurations sampled from 102 elements	2 306	6 918
	MC3D-extended	Extended MC3D crystals covering 93 elements with $Z < 100$	11 562	442 266
	MC3D-random-extended	Atomic species randomized over 102 elements in MC3D structures	5 397	54 472
	binary-random	Binary FCC and BCC random decorations over 102 elements	73 584	201 958
Total MAD-1.5			216 803 3 272 044	

TABLE I. Composition of the MAD-1.5 dataset. Original MAD-1 dataset is augmented with isolated atoms, dimers, trimers, extended and randomized crystals, and randomized binary structures to systematically expand chemical and configurational diversity up to 102 elements. The total number of structures and atoms across all subsets is reported in the last row.

mental pairings. We exclude larger distances because of the known self-interaction and static-correlation issues of non-spin polarized DFT for open-shell systems in this regime [20, 21]. The inclusion of these isolated dimers contributes to a reliable prediction of short-range repulsive interactions and low-coordination bonding environments that are under-represented in extended structures, particularly for element combinations that rarely occur in experimentally observed compounds.

The *trimers* subset extends this coverage to three-body interactions by generating configurations of three randomly selected atoms. For each trimer, three elements are chosen uniformly at random from the 102 available, and their positions are sampled such that the distance between any pair of atoms is no less than 0.25 times the sum of their covalent radii and no greater than the sum. These criteria are modified for hydrogen-hydrogen pairs (minimum distance set to 0.35 times the sum of covalent radii) and for heavy elements with atomic number $Z \geq 97$ (where a fixed covalent radius of 1.6 Å is assumed when paired with lighter elements). Configurations are generated stochastically until a representative set of unique trimers is obtained, ensuring diverse sampling of three-body geometries and angular arrangements. Together, the dimers and trimers subsets provide explicit low-body-order references that anchor the model’s representation of fundamental interatomic interactions, complementing the higher-body-order environments present in bulk, surface, and molecular configurations.

Overall, MAD-1.5 combines the diversity of MAD-1 with targeted structural enrichment and the improvement of the level of reference DFT theory, resulting in a dataset that offers broad chemical coverage across the full periodic table, compact in size, but rich in chemical information.

B. Electronic-structure details

All calculations were performed with FHI-aims [22] (version 250806), an all-electron, numeric atom-centered orbital (NAO) electronic-structure code [23]. Its use of real-space NAOs enable efficient scaling to large systems and the seamless treatment of both periodic and non-periodic structures, which is essential for the heterogeneous material classes in MAD-1.5. The input parameters are standardized across the dataset, enforcing consistency on the results. As the exchange–correlation functional, we opt for the meta-GGA r²SCAN [12, 13]. This functional improves accuracy significantly in comparison to the GGAs used in most of the available DFT datasets (including the original MAD-1 dataset), while keeping the computational cost affordable. In particular, r²SCAN was shown to vastly improve formation enthalpies of a wide range of solids [15] and, like SCAN, improve the description of hydrogen-bonds [14, 24] with respect to GGAs.

To achieve robust convergence, we employ an 8 Å⁻¹ k-point density grid (for periodic systems) and a Gaussian electronic smearing of 0.05 eV. We enforce convergence thresholds for the self-consistent solution of the Kohn–Sham equations of 10⁻⁶ eV for the energy, 10⁻⁴ eV/Å for the forces, and 10⁻⁵ e·a₀⁻³ for the electron density. FHI-aims “tight” basis sets and numerical settings are used for all elements. Species defaults (2020 version) provided by FHI-aims are used throughout, with a slight modification: For a subset of lanthanide and actinide elements (Pr–Yb, Pu–No, excluding Ce), we removed the confined 5d/6d function because, although physically motivated, they were found to hinder SCF convergence in non-spin-polarized calculations. This choice has limited impact on the accuracy of the resulting energies and forces. Each calculation outputs total energies, atomic forces, and stress tensors for periodic systems. We

Subset	Heuristic filter	LLPR filter
MC3D	33 357	33 343
MC3D-rattled	29 228	29 214
MC3D-random	2 117	2 075
MC3D-surface	4 958	4 928
MC3D-cluster	8 981	8 651
MC2D	2 529	2 502
SHIFTML-molcryst	8 574	8 572
SHIFTML-molfrags	3242	—
monomers	102	—
dimers	34 215	31 325
trimers	2 481	2 306
MC3D-extended	11 679	11 562
MC3D-random-ext.	5 574	5 397
binary-random	78 010	73 584
Total	225 047	216 803

TABLE II. MAD-1.5 subsets counts after successive outlier detection steps. Heuristic-based cleaning removed all structures with force magnitudes > 100 eV/Å. LLPR-uncertainty-based cleaning involved training and calibrating a LLPR model on the heuristically-cleaned dataset, and further eliminates the structures for which the actual absolute error in energy prediction was 3 times higher than the predicted energy uncertainty. A dash ‘—’ in the LLPR column indicates no change due to LLPR-based cleaning.

emphasize that using non-spin-polarized calculations neglects important physical effects, and affects the accuracy and numerical stability of calculations, e.g. for f -block elements and for dissociation curves. As for the MAD-1 dataset, we maintain that in the absence of a universally applicable DFT framework that converges reliably to the ground state of arbitrary materials, internal consistency has to be prioritized when building a dataset that strives to be truly universal.

C. Outlier detection

Achieving consistent DFT targets at the r²SCAN meta-GGA level across a large dataset of 102 elements is highly non-trivial, primarily due to degeneracies in self-consistent field (SCF) calculations and the sensitivity of this functional to integration grids [13]. These issues increase the risk of obtaining DFT ground states that do not converge or that converge to a local minimum, leading to substantial differences in calculated targets in repeated runs.

In order to mitigate this effect during model training, we performed a two-step cleaning procedure of the initial dataset of successfully converged calculations. First, we applied a heuristic-based cleaning, similar to that we used for MAD-1 [25]. We filtered out all structures with force magnitudes greater than 100 eV/Å to prevent overfitting on energies dominated by short-range repulsive contributions. Next, we used an uncertainty-based algorithm to eliminate potentially inconsistent structures with low

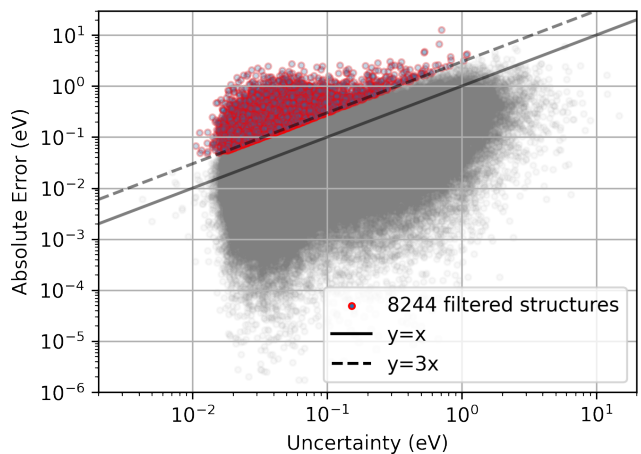


FIG. 2. Visualization of the dataset cleaning based on predicted LLPR uncertainties. All the structures for which the actual absolute error in energy predictions is 3 times higher than the predicted energy uncertainty are filtered out. A total of 8 244 structures filtered from the pre-cleaned version of the dataset are marked with red circles. The rest of the dataset is represented with gray dots.

predicted uncertainty and high actual error, following a procedure similar to that used in Ref. 26 to remove poorly converged chemical shielding calculations. To accomplish this, we trained the preliminary ML potential on the heuristically cleaned dataset from the previous step, and we calibrated a LLPR energy uncertainty estimate on the same training data (using a S-size model, see Section III A and Section III B for details). We then filtered out all structures for which the predicted energy uncertainty was 3 times lower than the actual error. A visualization of the LLPR selection process is shown in Figure 2. The overall statistics on the subsets counts before and after the cleaning is shown in Table II. We also distribute the set of structures that have been discarded by the LLPR cleaning procedure, both to compare with other dataset normalization protocols, and as they are likely to constitute challenging cases to stress-test the convergence of DFT implementations.

III. MODELS AND BENCHMARKS

A. Model architecture and training

To demonstrate the accuracy that can be achieved using a diverse, internally consistent dataset, we train a machine-learning interatomic potential based on the the *Point Edge Transformer* (PET) [27, 28]. PET is a rotationally unconstrained, transformer-based graph neural network (GNN) designed to predict the properties of atomistic systems with high accuracy and computational efficiency. The model predicts energies as a sum of atomic contributions. Conservative forces and stresses are com-

Model	PET-MAD-1.5-XS	PET-MAD-1.5-S
Trained from	PET-OMat-XS	PET-OMat-S
Parameter count	4.5M	25.9M
Edge features	128	256
GNN layers	2	3
Attention layers	1	1
Cutoff radius (Å)	7.5	8.0
Adaptive # neighbors	8	16
Max learning rate	2e-4	1e-4
Batch size	256	256
Number of epochs	200	200
Weight decay	1e-5	1e-5
E loss weight	10.0	10.0
F loss weight	1.0	1.0
S loss weight	1.0	1.0
NC F loss weight	0.1	0.1
NC S loss weight	0.1	0.1

TABLE III. Model and training hyperparameters for the models evaluated in this work. Two model sizes of the PET-MAD-1.5 (XS and S) were trained from the corresponding OMat checkpoints from the Ref. 28. The number of node features corresponds to four times that of edge features for all models. In all cases, a linear learning rate warm-up of 10% of the total number of epochs was performed, followed by cosine learning rate annealing, which starts from the maximum value and decays to zero at the end of training. Both r²SCAN and PBE targets were trained with the same weights for energies (E), forces (F), stresses (S), non-conservative forces (NC F) and non-conservative stresses (NC S) in the loss function.

puted using automatic differentiation as derivatives of the total energy prediction with respect to atomic positions and strain tensors, respectively. We use separate heads to predict non-conservative forces and stresses, which can be used to accelerate simulations [29]. We refer the reader to Ref. 28, that discusses the specific architecture we use here, including an adaptive cutoff approach that allows to achieve a balanced description of systems of widely different density. In fact, the PET-MAD-1.5 models presented in this work are fine-tuned from those trained in Ref. 28 on the OMat24 dataset [30], and they therefore match the XS and S sizes of the models presented there.

All the models were trained on a cleaned version of the MAD-1.5 dataset (cleaning details are provided in Sec. II C), targeting the atomization energy of each system - i.e. the quantity left after subtracting stoichiometric monomer energies from the total energy, atomic forces and, where applicable, stresses. The dataset was split into training, validation, and test subsets comprising roughly 80%, 10%, and 10% of the total number of cleaned structures, respectively, using a stratified split method. Since dimers and trimers define the fundamental two- and three-body interactions and, together with monomers, the zero-density limit of the potential, inserting these structures in the training set ensures physically correct short- and long-range behavior and prevents the model from compensating errors through spurious

many-body correlations [31]. Like monomers, these low-order clusters are not included to benchmark generalization; rather, they are incorporated as physical constraints in the training split, increasing its relative size to 83%. We observed that including a separate head targeting a lower level of theory improves the force accuracy of the fine-tuned model by approximately 25% - possibly by further reducing the impact of some residual inconsistencies of the harder-to-converge r²SCAN functional and/or the mismatch in level of theory with the pre-trained model. For this reason, we also used a subset of the MAD-1.5 dataset, that we obtained using the PBE functional [32] during early phases of dataset construction, split in accordance with the cross-validation subsets mentioned above. These data are targeted with separate, PBE-specific heads and equivalent loss weightings as described in Table III. Given that this dataset has a lower level of theory, and it is not as carefully curated as MAD-1.5, we discard the PBE heads from the models after training. The training runs were performed using the `metatrain` package [33] based on PyTorch [34] using 16 NVIDIA GH200 GPUs. Training times were approximately 16 and 23 hours for the XS and S sizes, respectively. All the hyperparameters used during model selection and training are listed in Table III. Weight optimization was performed using the AdamW optimizer [35] with a weight decay of 10⁻⁵ combined with the cosine annealing learning rate scheduler [36] and a linear learning rate warm-up for the first 10% of the total number of epochs. Prior to training, targets are normalized in the following ways: 1) a further dataset-dependent chemical composition-based contribution is subtracted from the atomization energies, and 2) targets are scaled by dividing each by their standard deviation across the training set. The loss function was based on a weighted sum of the root-mean-squared errors for each predicted target. Non-conservative heads for direct forces and stresses predictions were trained along with their conservative counterparts for both r²SCAN and PBE heads with a reduced weight in the loss function, in order to enable accelerated inference [29]. The loss weightings of each target are provided in Table III.

B. Uncertainty quantification

We provide built-in machine-learning uncertainties for our models using the last-layer prediction rigidity (LLPR) method [37]. Within the LLPR formalism, the uncertainty of the model’s prediction in total energy is computed as

$$\sigma^2 = \alpha^2 \mathbf{x}^\top (\mathbf{X}^\top \mathbf{X} + \zeta^2 \mathbf{I})^{-1} \mathbf{x}, \quad (1)$$

where σ is the predictive uncertainty, \mathbf{x} are the last-layer features associated to the predicted sample, \mathbf{X} is a matrix whose rows correspond to the last-layer features of all samples in the training set, ζ^2 is a small positive regularization parameter, and the calibration factor α^2 is

Subset	PET-MAD-1.5-XS		PET-MAD-1.5-S	
	E	\mathbf{f}	E	\mathbf{f}
MC3D	12.16	62.80	4.07	24.21
MC3D-rattled	13.01	161.99	4.47	69.06
MC3D-random	45.09	190.05	30.14	92.54
MC3D-surface	19.08	117.84	5.49	51.93
MC3D-cluster	19.43	120.31	11.14	69.28
MC2D	18.51	68.93	6.22	32.17
SHIFTML-molcryst	4.91	60.69	1.83	24.30
SHIFTML-molfrags	7.63	52.87	2.45	23.94
MC3D-extended	18.83	74.37	11.11	30.03
binary-random	23.57	32.53	16.91	17.77
MC3D-random-ext.	41.43	213.13	30.64	119.02
Total	18.73	86.45	11.09	36.81

TABLE IV. Performance of the PET-MAD-1.5 models on the subset-resolved MAD-1.5 test set. Mean absolute error (MAE) in energy | forces prediction is given in meV/atom | meV/Å.

determined on a calibration set. Given that the last-layer features have to be computed and materialized during the model’s forward pass, this uncertainty quantification method adds negligible overhead to its predictions. Beyond predictive uncertainties, this construction allows users to compute a range of local and global rigidity measures [38, 39]. The LLPR covariance matrix $\mathbf{X}^\top \mathbf{X}$ is also used to sample the members of a last-layer ensemble as described in Ref. [37]. This further allows the propagation of uncertainties through arbitrarily complex workflows [4, 40] when using our models.

C. Benchmarking

Since MAD-1.5 consists of a diverse set of material classes, with systems that span different sizes, dimensionalities and chemistries, its performance on a test subset can serve a first, simple measure of its expected accuracy for different types of problems. A subset-resolved analysis of each model’s errors is shown in Table IV. As expected, the S-size model achieves much greater accuracy than the XS model, with an excellent mean absolute force error (MAE) value of 37 meV/Å. Even though this value is dominated by large and low-error subsets like *MC3D* or *binary-random*, it still does not exceed 70 meV/Å for all “reasonable” configurations, and only reaches 120 meV/Å on the *MC3D-random-extended* subset. Although the XS model has a roughly five times smaller number of parameters, it still achieves a level of accuracy that is comparable to that of the original PET-MAD-1, while covering a larger chemical space and having up to 3 times lower inference time compared to its S-size analog. Figure IIIB shows timings of the models for a few different kinds of materials in both the ASE [41] and LAMMPS [42] implementations, while also including a comparison with the original implementation

Subset	v1.5-XS (this work)		v1.5-S (this work)		v1.0.2 (Ref. 4)	
	E	\mathbf{f}	E	\mathbf{f}	E	\mathbf{f}
MAD-1	12.43	76.60	4.29	31.88	17.6	65.1
MPtrj	22.43	118.07	7.65	50.80	22.3	77.9
MatBench	36.86	82.37	14.66	38.21	31.3	—
Alexandria	49.83	80.05	21.11	39.84	49.0	66.8
OC2020	27.32	150.57	7.51	70.53	18.3	114.5
SPICE	9.84	72.99	3.90	36.96	3.7	59.5
MD22	9.45	84.53	6.12	43.79	1.9	65.6

TABLE V. Performance of the PET-MAD-1.5 models on the subset-resolved MADBench benchmark. Mean absolute error (MAE) in energy and forces prediction is given in meV/atom and meV/Å, respectively. Results of the PET-MAD-1 (v1.0.2) trained on the original PBEsol version of the MAD-1 dataset from Ref. 4 are provided for comparison. Each model is evaluated against a set of consistently computed DFT targets corresponding to those used for training. The results of the best model for each subset are highlighted in bold.

used in PET-MAD-1.

In addition to the in-domain evaluation on a test subset, we performed an out-of-domain (OOD) analysis of the models’ performance using a MADBench benchmark - a minimalistic set of configurations sampled from various datasets used for atomistic machine learning from Ref. 4. The main advantage of this benchmark is the availability of targets computed consistently with various DFT settings. This allows for direct comparison of the models, ensuring that discrepancies are not caused by significant differences in the reference data. We recomputed the target energies and forces on the MADBench configurations using the same DFT setup as for the MAD-1.5 calculations, and evaluated the PET-MAD-1.5 models against them. The subset-resolved analysis of the models’ errors is provided in Table V. Even though only the MAD subset of the MADBench can be considered as a pure in-domain part of the benchmark, both XS- and S-size models show good accuracies on the other OOD subsets, while the latter gets a substantial improvement over the original PET-MAD-1 model. Similar to the evaluation on a test subset, the errors on forces do not exceed 70 meV/Å, indicating the model’s excellent generalizability.

We note, that these results are unprecedented, especially given that our models (1) cover a very large chemical space and (2) target the r²SCAN level of theory. Massive datasets of several million structures are practically unavailable for this level of theory due to the increased cost and lower robustness of meta-GGA DFT. The high accuracy of the models we propose is striking when compared, for instance, to the largest models trained on OMat24 (which achieve around 45-50 meV/Å [28] on a massive PBE dataset), MAD-1 (around 70-75 meV/Å [4], PBEsol), or MATPES (>100 meV/Å [10], both in its PBE and r²SCAN versions). Compared to these test sub-

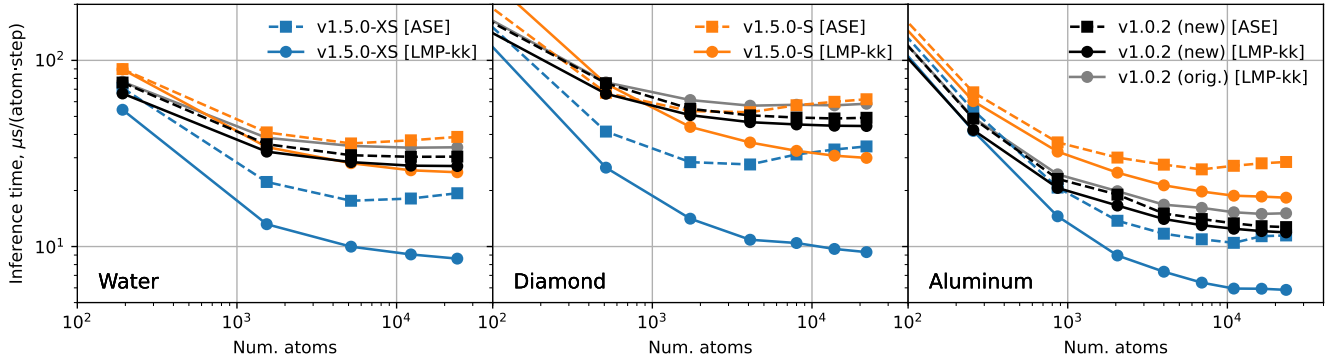


FIG. 3. Inference time of PET-MAD universal models evaluated over different kinds of materials and varying system sizes. The results of the XS- and S-size PET-MAD-1.5 models is shown with blue and orange lines, respectively, where circle and square markers are denoting the ASE [41] and LAMMPS (with Kokkos backend) [42, 43] implementations. The original PET-MAD-1 timings with both the model weights and code implementations from Ref. 4 are shown with gray lines. The PET-MAD-1 timings with the updated code implementation associated with the PET-MAD-1.5 release are shown in black. All performance test were done on a single NVIDIA H100 GPU. Conservative heads were used for all the predictions.

set results, our models achieve a MAE of $86 \text{ meV}/\text{\AA}$ and $37 \text{ meV}/\text{\AA}$ in forces prediction for the XS and S sizes, respectively. Covering such a large chemical space at a high level of theory and accuracy is made possible by predominantly two facts: first, our models are pre-trained on the extensive OMat24 dataset, which allows for the creation of high-quality neural representations. Second, they are fine-tuned on the smaller, but accurate and carefully curated MAD-1.5 dataset, which maintains a high level of internal consistency in the underlying DFT, and therefore avoids unlearnable noise in target data that would deteriorate the models’ accuracy. Last, but not the least, both new models are fast, with S-sized models being comparable to PET-MAD-1.0 and XS models being much faster (Fig. III B).

D. Mendeleev clusters

As a challenging test of the stability of the potential, we set up the following benchmark simulations, inspired by similar simulations performed by some of us for high-entropy alloys [44, 45]. We generate “Mendeleev clusters” by creating a $3 \times 3 \times 3$ *fcc* box, and assign at random to each site one of the atoms in the periodic table, leaving six vacancies to avoid repetitions. The initial structure is relaxed, keeping the cell cubic, and the boundary conditions then extended to a side of 40 \AA , effectively creating an initial particle with a cubic shape. This procedure is repeated to create 16 structures, each of which is used as the initial configuration in a replica exchange molecular dynamics (REMD) simulation, with replicas at temperatures between 300 K and 3000 K , uniformly spaced on a logarithmic scale, using the implementation in i-PI [46, 47] and the PET-MAD-1.5-S model. We run 100 ps -long trajectories in the *NVT* ensemble, us-

ing an efficient thermostat combining a stochastic velocity rescaling[48] and an optimal-sampling Generalized Langevin Equation thermostat[49]. We also attempt, every two steps, a random exchange between the position of two atoms, to accelerate the exploration of configuration space.

This is an incredibly challenging setup, probing high temperatures, atoms in bulk, surface and (potentially) gas phase environments, and efficient sampling to maximize the possibility of encountering unphysical low-energy minima. The PET-MAD-1.5-S potential generates stable trajectories, resulting in a compact quasi-spherical particle that has expelled all and only the noble gases for the low-temperature replicas, while at the highest temperature the surface of the cluster becomes irregular, and one can find occasionally isolated atoms of other elements, as well as alkali halide dimers (Figure 4). To provide a more quantitative assessment of the reliability of PET-MAD-1.5-S in this extreme regime, we performed single-point $r^2\text{SCAN}$ calculations for some of the final structures obtained from the REMD trajectory. The convergence of these calculations is extremely challenging, requiring careful tuning of the self-consistency loop and a relaxation of the convergence threshold. Even though this indicates that the DFT reference may itself be affected by a degree of uncertainty, the comparison between the electronic-structure calculations and PET-MAD predictions is reassuring, with a force error around $150 \text{ meV}/\text{\AA}$ (Figure 4, bottom), in line with the validation error on the *MC3D-random-extended* subset, and lower than the errors that first-generation MLIPs would yield for single-component bulk materials [50].

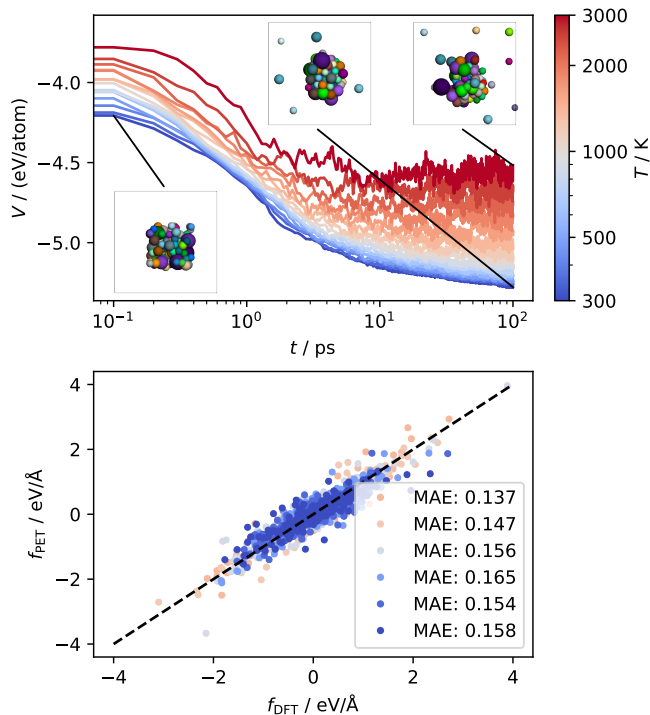


FIG. 4. (top) Time series of the potential energy for the re-ordered temperature replicas for a REMD simulation of a Mendeleev cluster containing 102 elements. Insets show the initial and final structures of the 300 K replica, and the final structure of the 3000 K replica. Isolated atoms in the end of the simulation are typically either noble gases or elements with a high vapor pressure (such as Hg). (bottom) Parity plot of the force components for the final structures in the simulation, color-coded based on the target temperature, comparing the values obtained with PET-MAD-1.5-S with those computed with single-point DFT calculations. Typical errors are of the order of 150 meV/Å MAE.

IV. CONCLUSIONS

We present MAD-1.5, a dataset designed to cover the entire periodic table up to No, which includes all isotopes with a half-life above a day, covering organic and inorganic materials, bulk structures, surfaces, clusters and molecules. In line with the design principle of “massive atomic diversity”, MAD-1.5 contains about 200’000 structures, chosen to be representative of realistic materials and molecules, but to also include very high-energy artificial structures.

We use reference calculations that are highly converged, based on the all-electron numeric atomic orbitals code FHI-aims, and use the r²SCAN meta-GGA functional to strike a good balance between computational cost and accuracy. We further improve the internal consistency of MAD-1.5 by performing an outlier screening procedure based on the calculation of last-layer rigidity uncertainties. We also make available the structures that are discarded for having a very large empirical error-to-

uncertainty ratio, as they are likely to represent hard-to-converge benchmarks for DFT calculations.

Based on the cleaned MAD-1.5 dataset, we train demonstrative models based on the unconstrained PET architecture. PET-MAD-1.5-XS and PET-MAD-1.5-S achieve excellent performance compared to models that are practically usable for advanced materials simulations, while covering a much larger portion of chemical space. Besides being accurate in benchmarks, PET-MAD-1.5 models are also extremely stable. We introduce a “Mendeleev cluster” stress test that consists in simulating a nanoparticle containing one each of all the elements present in MAD-1.5 across a broad range of temperatures. The simulation remains stable over a collective 1.6 ns of trajectory, and lead to physically plausible outcomes and an error of about 150 meV/Å relative to explicit electronic-structure calculations. This is possibly the most compelling demonstration of the universal applicability of PET-MAD-1.5, that in turns showcases the effectiveness of a dataset construction strategy focused on diversity and internal consistency of the electronic-structure calculations.

V. DATA RECORD AND MODEL AVAILABILITY

The MAD-1.5 dataset is made publicly available as a record [51] within the Materials Cloud Archive [52], which is a FAIR repository dedicated to materials-science simulations. Structures and targets computed at r²SCAN and PBE levels of theory that comprise the dataset are provided in extended XYZ format. Energies (specifically total energy under key `energy`, and atomization energy under key `atomization_energy`), stresses (`stress`), and lattice parameters (`Lattice`) are stored in the file headers, and atom types (`species`), positions (`pos`), and forces (`forces`) are stored as space-separated entries. Cartesian coordinates, energies, forces, and stresses are given in Å, eV, eV/Å, and eV/Å³, respectively. Also stored in the header are the name of the subset to which each structure belongs (`subset`) and the numeric index of the structure within its subset (`frame_id`). Together these uniquely identify each structure in the dataset.

Specifically, the record contains:

- *mad-1.5-r2scan-train.xyz* - the training set used in model training.
- *mad-1.5-r2scan-val.xyz* - the validation set used in model training.
- *mad-1.5-r2scan-test.xyz* - the test set used in model evaluation.
- *mad-1.5-r2scan-llpr-rejected.xyz* - the 8244 structures removed by the LLPR uncertainty-based filtering procedure shown in Fig. 2.

- *mad-1.5-pbe.xyz* - the combined training, validation, and test splits (consistent with the r²SCAN splits) of a subset of MAD-1.5 computed with the PBE functional, used in model training.

We also release PET-MAD-1.5 as two foundation MLIPs with varying number of parameters, trained on the above data splits. These are available in the public GitHub repository <https://github.com/lab-cosmo/upet>. An example to reproduce the simulation of the Mendeleev cluster with these (and other) universal MLIPs can be found at <https://atomistic-cookbook.org/examples/mendeleev/mendeleev.html>.

VI. AUTHOR CONTRIBUTIONS

C.M. performed the electronic-structure calculations for the MAD-1.5 dataset, generated the *MC3D-random-extended* dataset and relaxed part of the *MC3D-extended* subset. C.M. and P.L. generated the *monomer*, *dimer*, and *trimer* subsets. P.P. generated the *binary-random* subset. A.M. trained the PET-MAD-1.5-S and PET-MAD-1.5-XS models, carried out the uncertainty quantification protocol used to identify outliers, ran the accuracy and speed benchmark evaluations, and managed the model distribution. F.B. trained preliminary models and provided support in model training. A.M. and F.B. managed the UPET repository and PET model code implementation. J.W.A. provided technical support for the initial setup of the electronic-structure calculations and curated the data distribution on Materials Cloud. M.R. and C.M. addressed convergence issues for struc-

tures containing d- and f-block elements. M.R. provided technical support for the electronic-structure calculations and performed the electronic-structure calculations for the Mendeleev cluster. A.M. organized and managed the technical part of the project. M.C. supervised and guided the project and performed the REMD simulations. All authors contributed to the writing and revision of the manuscript.

ACKNOWLEDGMENTS

The Authors are grateful to Damien K. J. Lee for providing template orderings of the crystal structures used for the *binary-random* subset generation and to Marnik Bercx, Sebastian Huber and Giovanni Pizzi for providing the initial configurations for the *MC3D-extended* subset of MAD-1.5. A.M. was supported by an Industrial Grant from BASF. P.L., P.P. and M.C. acknowledge support by the NCCR MARVEL, funded by the Swiss National Science Foundation (SNSF, grant number 182892). F.B. was supported by a grant from the Platform for Advanced Scientific Computing (PASC) and the Swiss AI Initiative (2025 Fellowship Program). J.W.A. and M.C. received funding from the European Research Council (ERC) under the European Union’s Horizon 2020 research and innovation programme (grant agreement No. 101001890 - FIAMMA). M.R. and C.M. acknowledge computer time at the Max Planck Computing and Data Facility (MPCDF). C.M., F.B., P.P., J.W.A., P.L., M.C. and A.M. acknowledge Alps and Eiger at the Swiss National Supercomputing Center, Switzerland with project ID lp133 on Daint and ID mr31 under MARVEL’s share on Eiger, as well as the SCITAS platform at EPFL.

-
- [1] J. Behler, Perspective: Machine learning potentials for atomistic simulations, *The Journal of Chemical Physics* **145**, 10.1063/1.4966192 (2016).
 - [2] F. L. Thiemann, N. O’Neill, V. Kapil, A. Michaelides, and C. Schran, Introduction to machine learning potentials for atomistic simulations, *Journal of Physics: Condensed Matter* **37**, 073002 (2024).
 - [3] R. Jacobs, D. Morgan, S. Attarian, J. Meng, C. Shen, Z. Wu, C. Y. Xie, J. H. Yang, N. Artrith, B. Blaiszik, G. Ceder, K. Choudhary, G. Csanyi, E. D. Cubuk, B. Deng, R. Drautz, X. Fu, J. Godwin, V. Honavar, O. Isayev, A. Johansson, B. Kozinsky, S. Martiniani, S. P. Ong, I. Poltavsky, K. Schmidt, S. Takamoto, A. P. Thompson, J. Westermayr, and B. M. Wood, A practical guide to machine learning interatomic potentials – status and future, *Current Opinion in Solid State and Materials Science* **35**, 101214 (2025).
 - [4] A. Mazitov, F. Bigi, M. Kellner, P. Pegolo, D. Tisi, G. Fraux, S. Pozdnyakov, P. Loche, and M. Ceriotti, Petmad as a lightweight universal interatomic potential for advanced materials modeling, *Nature Communications* **16**, 10653 (2025).
 - [5] A. Mazitov, S. Chorna, G. Fraux, M. Bercx, G. Pizzi, S. De, and M. Ceriotti, Massive atomic diversity: a compact universal dataset for atomistic machine learning, *Scientific Data* **12**, 10.1038/s41597-025-06109-y (2025).
 - [6] H.-C. Wang, S. Botti, and M. A. Marques, Predicting stable crystalline compounds using chemical similarity, *npj Computational Materials* **7**, 12 (2021).
 - [7] J. Schmidt, T. F. Cerqueira, A. H. Romero, A. Loew, F. Jäger, H.-C. Wang, S. Botti, and M. A. Marques, Improving machine-learning models in materials science through large datasets, *Materials Today Physics* **48**, 101560 (2024).
 - [8] L. Barroso-Luque, M. Shuaibi, X. Fu, B. M. Wood, M. Dzamba, M. Gao, A. Rizvi, C. L. Zitnick, and Z. W. Ulissi, Open materials 2024 (omat24) inorganic materials dataset and models, arXiv preprint arXiv:2410.12771 (2024).
 - [9] D. S. Levine, M. Shuaibi, E. W. C. Spotte-Smith, M. G. Taylor, M. R. Hasyim, K. Michel, I. Batatia, G. Csányi, M. Dzamba, P. Eastman, *et al.*, The open molecules 2025 (omol25) dataset, evaluations, and models, arXiv preprint arXiv:2505.08762 (2025).

- [10] A. D. Kaplan, R. Liu, J. Qi, T. W. Ko, B. Deng, J. Riebesell, G. Ceder, K. A. Persson, and S. P. Ong, A foundational potential energy surface dataset for materials, arXiv preprint arXiv:2503.04070 (2025).
- [11] J. P. Perdew, A. Ruzsinszky, G. I. Csonka, O. A. Vydrov, G. E. Scuseria, L. A. Constantin, X. Zhou, and K. Burke, Restoring the Density-Gradient Expansion for Exchange in Solids and Surfaces, *Phys. Rev. Lett.* **100**, 136406 (2008).
- [12] J. Sun, A. Ruzsinszky, and J. P. Perdew, Strongly constrained and appropriately normed semilocal density functional, *Physical Review Letters* **115**, 10.1103/physrevlett.115.036402 (2015).
- [13] J. W. Furness, A. D. Kaplan, J. Ning, J. P. Perdew, and J. Sun, Accurate and numerically efficient r2scan meta-generalized gradient approximation, *The Journal of Physical Chemistry Letters* **11**, 8208–8215 (2020).
- [14] J. Sun, R. C. Remsing, Y. Zhang, Z. Sun, A. Ruzsinszky, H. Peng, Z. Yang, A. Paul, U. Waghmare, X. Wu, M. L. Klein, and J. P. Perdew, Accurate first-principles structures and energies of diversely bonded systems from an efficient density functional, *Nature Chemistry* **8**, 831 (2016).
- [15] M. Kothakonda, A. D. Kaplan, E. B. Isaacs, C. J. Bartel, J. W. Furness, J. Ning, C. Wolverton, J. P. Perdew, and J. Sun, Testing the r2scan density functional for the thermodynamic stability of solids with and without a van der waals correction, *ACS Materials Au* **3**, 102 (2023), <https://doi.org/10.1021/acsmaterialsau.2c00059>.
- [16] H. Liu, X. Bai, J. Ning, Y. Hou, Z. Song, A. Ramasamy, R. Zhang, Y. Li, J. Sun, and B. Xiao, Assessing r2scan meta-gga functional for structural parameters, cohesive energy, mechanical modulus, and thermophysical properties of 3d, 4d, and 5d transition metals, *The Journal of Chemical Physics* **160**, 10.1063/5.0176415 (2024).
- [17] S. P. Huber, M. Minotakis, M. Bercx, T. Reents, K. Eimre, N. Paulish, N. Hörmann, M. Uhrin, N. Marzari, and G. Pizzi, Mc3d: the materials cloud computational database of experimentally known stoichiometric inorganics, *Digital Discovery* 10.1039/d5dd00415b (2026).
- [18] G. L. W. Hart and R. W. Forcade, Algorithm for generating derivative structures, *Physical Review B* **77**, 10.1103/physrevb.77.224115 (2008).
- [19] S. K. Kollí, A. R. Natarajan, J. C. Thomas, T. M. Pollock, and A. Van der Ven, Discovering hierarchies among intermetallic crystal structures, *Phys. Rev. Mater.* **4**, 113604 (2020).
- [20] A. J. Cohen, P. Mori-Sánchez, and W. Yang, Insights into current limitations of density functional theory., *Science* **321**, 792 (2008), 18687952.
- [21] K. R. Bryenton, A. A. Adeleke, S. G. Dale, and E. R. Johnson, Delocalization error: The greatest outstanding challenge in density-functional theory, *Wiley Interdisciplinary Reviews: Computational Molecular Science* **13**, e1631 (2023).
- [22] V. Blum, R. Gehrke, F. Hanke, P. Havu, V. Havu, X. Ren, K. Reuter, and M. Scheffler, Ab initio molecular simulations with numeric atom-centered orbitals, *Computer Physics Communications* **180**, 2175 (2009).
- [23] J. W. Abbott, C. M. Acosta, A. Akkoush, A. Ambrosetti, V. Atalla, A. Bagrets, J. Behler, D. Berger, B. Bieniek, J. Björk, V. Blum, S. Bohloul, C. L. Box, N. Boyer, D. S. Brambila, G. A. Bramley, K. R. Bryenton, M. Camarasa-Gómez, C. Carbogno, F. Caruso, S. Chutia, M. Ceriotti, G. Csányi, W. Dawson, F. A. Delesma, F. Della Sala, B. Delley, R. A. DiStasio, Jr., M. Dragoumi, S. Driessen, M. Dvorak, S. Erker, F. Evers, E. Fabiano, M. R. Farrow, F. Fiebig, J. Filser, L. Foppa, L. Gallandi, A. Garcia, R. Gehrke, S. Ghan, L. M. Ghiringhelli, M. Glass, S. Goedecker, D. Golze, M. Gramzow, J. A. Green, A. Grisafi, A. Grüneis, J. Günzl, S. Gutzeit, S. J. Hall, F. Hanke, V. Havu, X. He, J. Hekele, O. Hellman, U. Herath, J. Hermann, D. Hernangómez-Pérez, O. T. Hofmann, J. Hoja, S. Hollweger, L. Hörmann, B. Hourahine, W. B. How, W. P. Huhn, M. Hülsberg, T. Jacob, S. P. Jand, H. Jiang, E. R. Johnson, W. Jürgens, J. M. Kalk, Y. Kanai, K. Kang, P. Karpov, E. Keller, R. Kempt, D. Khan, M. Kick, B. P. Klein, J. Kloppenburg, A. Knoll, F. Knoop, F. Knuth, S. S. Köcher, J. Kockläuner, S. Kokott, T. Körzdörfer, H.-H. Kowalski, P. Kratzer, P. Küs, R. Laasner, B. Lang, B. Lange, M. F. Langer, A. H. Larsen, H. Lederer, S. Lehtola, M.-O. Lenz-Himmer, M. Leucke, S. Levchenko, A. Lewis, O. A. von Lilienfeld, K. Lion, W. Lipsunen, J. Lischner, Y. Litman, C. Liu, Q.-L. Liu, A. J. Logsdail, M. Lorke, Z. Lou, I. Mandzhieva, A. Marek, J. T. Margraf, R. J. Maurer, T. Melson, F. Merz, J. Meyer, G. S. Michelitsch, T. Mizoguchi, E. Moerman, D. Morgan, J. Morgenstein, J. Moussa, A. S. Nair, L. Nemeč, H. Oberhofer, A. Otero-de-la Roza, R. L. Panadés-Barrueta, T. Patlolla, M. Pogodaeva, A. Pöpl, A. J. A. Price, T. A. R. Purcell, J. Quan, N. Raimbault, M. Rampp, K. Rasim, R. Redmer, X. Ren, K. Reuter, N. A. Richter, S. Ringe, P. Rinke, S. P. Rittmeyer, H. I. Rivera-Arrieta, M. Ropo, M. Rossi, V. Ruiz, N. Rybin, A. Sanfilippo, M. Scheffler, C. Scheurer, C. Schober, F. Schubert, T. Shen, C. Shepard, H. Shang, K. Shibata, A. Sobolev, R. Song, A. Soon, D. T. Speckhard, P. V. Stishenko, M. Tahir, I. Takahara, J. Tang, Z. Tang, T. Theis, F. Theiss, A. Tkatchenko, M. Todorović, G. Trenins, O. T. Unke, A. Vázquez-Mayagoitia, O. van Vuren, D. Waldschmidt, H. Wang, Y. Wang, J. Waeferink, J. Wilhelm, S. Woodley, J. Xu, Y. Xu, Y. Yao, Y. Yao, M. Yoon, V. W.-z. Yu, Z. Yuan, M. Zacharias, I. Y. Zhang, M.-Y. Zhang, W. Zhang, R. Zhao, S. Zhao, R. Zhou, Y. Zhou, and T. Zhu, Roadmap on advancements of the FHI-aims software package (2025), arXiv:2505.00125.
- [24] M. Chen, H.-Y. Ko, R. C. Remsing, M. F. Calegari Andrade, B. Santra, Z. Sun, A. Selloni, R. Car, M. L. Klein, J. P. Perdew, and X. Wu, Ab initio theory and modeling of water, *Proceedings of the National Academy of Sciences* **114**, 10846–10851 (2017).
- [25] A. Mazitov, S. Chorna, G. Fraux, M. Bercx, G. Pizzi, S. De, and M. Ceriotti, Massive Atomic Diversity: A compact universal dataset for atomistic machine learning, *Sci Data* **12**, 1857 (2025).
- [26] F. M. Paruzzo, A. Hofstetter, F. Musil, S. De, M. Ceriotti, and L. Emsley, Chemical shifts in molecular solids by machine learning, *Nature Communications* **9**, 4501 (2018), arXiv:1805.11541.
- [27] S. Pozdnyakov and M. Ceriotti, Smooth, exact rotational symmetrization for deep learning on point clouds, *Advances in Neural Information Processing Systems* **36**, 79469 (2023).
- [28] F. Bigi, P. Pegolo, A. Mazitov, and M. Ceriotti, Pushing the limits of unconstrained machine-learned interatomic

- potentials, arXiv preprint arXiv:2601.16195 (2026).
- [29] F. Bigi, M. F. Langer, and M. Ceriotti, The dark side of the forces: Assessing non-conservative force models for atomistic machine learning, in *Forty-Second International Conference on Machine Learning* (2025).
- [30] L. Barroso-Luque, M. Shuaibi, X. Fu, B. M. Wood, M. Dzamba, M. Gao, A. Rizvi, C. L. Zitnick, and Z. W. Ulissi, Open materials 2024 (omat24) inorganic materials dataset and models, arXiv preprint arXiv:2410.12771 (2024).
- [31] S. Chong, T. Jiang, M. Domina, F. Bigi, F. Grasselli, J. Lee, and M. Ceriotti, Resolving the body-order paradox of machine learning interatomic potentials, *The Journal of Chemical Physics* **164**, 064121 (2026).
- [32] J. P. Perdew, K. Burke, and M. Ernzerhof, Generalized gradient approximation made simple, *Physical Review Letters* **77**, 3865–3868 (1996).
- [33] F. Bigi, J. W. Abbott, P. Loche, A. Mazitov, D. Tisi, M. F. Langer, A. Goscinski, P. Pegolo, S. Chong, R. Goswami, *et al.*, Metatensor and metatomic: foundational libraries for interoperable atomistic machine learning, arXiv preprint arXiv:2508.15704 (2025).
- [34] A. Paszke, S. Gross, F. Massa, A. Lerer, J. Bradbury, G. Chanan, T. Killeen, Z. Lin, N. Gimelshein, L. Antiga, A. Desmaison, A. Kopf, E. Yang, Z. DeVito, M. Raison, A. Tejani, S. Chilamkurthy, B. Steiner, L. Fang, J. Bai, and S. Chintala, PyTorch: An imperative style, high-performance deep learning library, in *Advances in Neural Information Processing Systems 32*, edited by H. Wallach, H. Larochelle, A. Beygelzimer, F. dAlché-Buc, E. Fox, and R. Garnett (Curran Associates, Inc., 2019) pp. 8024–8035.
- [35] I. Loshchilov and F. Hutter, Decoupled weight decay regularization, arXiv preprint arXiv:1711.05101 (2017).
- [36] I. Loshchilov and F. Hutter, Sgdr: Stochastic gradient descent with warm restarts, arXiv preprint arXiv:1608.03983 (2016).
- [37] F. Bigi, S. Chong, M. Ceriotti, and F. Grasselli, A prediction rigidity formalism for low-cost uncertainties in trained neural networks, *Machine Learning: Science and Technology* **5**, 045018 (2024).
- [38] S. Chong, F. Grasselli, C. Ben Mahmoud, J. D. Morrow, V. L. Deringer, and M. Ceriotti, Robustness of local predictions in atomistic machine learning models, *Journal of Chemical Theory and Computation* **19**, 8020 (2023).
- [39] S. Chong, F. Bigi, F. Grasselli, P. Loche, M. Kellner, and M. Ceriotti, Prediction rigidities for data-driven chemistry, *Faraday Discussions* **256**, 322 (2025).
- [40] M. Kellner and M. Ceriotti, Uncertainty quantification by direct propagation of shallow ensembles, *Machine Learning: Science and Technology* **5**, 035006 (2024).
- [41] A. Hjorth Larsen, J. Jørgen Mortensen, J. Blomqvist, I. E. Castelli, R. Christensen, M. Dulak, J. Friis, M. N. Groves, B. Hammer, C. Hargus, *et al.*, The atomic simulation environment—a python library for working with atoms, *Journal of Physics: Condensed Matter* **29**, 273002 (2017).
- [42] A. P. Thompson, H. M. Aktulga, R. Berger, D. S. Bolintineanu, W. M. Brown, P. S. Crozier, P. J. In’t Veld, A. Kohlmeyer, S. G. Moore, T. D. Nguyen, *et al.*, LAMMPS—a flexible simulation tool for particle-based materials modeling at the atomic, meso, and continuum scales, *Computer physics communications* **271**, 108171 (2022).
- [43] C. R. Trott, D. Lebrun-Grandié, D. Arndt, J. Ciesko, V. Dang, N. Ellingwood, R. Gayatri, E. Harvey, D. S. Hollman, D. Ibanez, N. Liber, J. Madsen, J. Miles, D. Poliakoff, A. Powell, S. Rajamanickam, M. Simberg, D. Sunderland, B. Turcksin, and J. Wilke, Kokkos 3: Programming model extensions for the exascale era, *IEEE Transactions on Parallel and Distributed Systems* **33**, 805 (2022).
- [44] N. Lopanitsyna, G. Fraux, M. A. Springer, S. De, and M. Ceriotti, Modeling high-entropy transition metal alloys with alchemical compression, *Phys. Rev. Materials* **7**, 045802 (2023).
- [45] A. Mazitov, M. A. Springer, N. Lopanitsyna, G. Fraux, S. De, and M. Ceriotti, Surface segregation in high-entropy alloys from alchemical machine learning, *J. Phys. Mater.* **7**, 025007 (2024).
- [46] R. Petraglia, A. Nicolaï, M. D. Wodrich, M. Ceriotti, and C. Corminboeuf, Beyond static structures: Putting forth REMD as a tool to solve problems in computational organic chemistry, *Journal of Computational Chemistry* **37**, 83 (2016).
- [47] Y. Litman, V. Kapil, Y. M. Y. Feldman, D. Tisi, T. Begušić, K. Fidanyan, G. Fraux, J. Higer, M. Kellner, T. E. Li, E. S. Pósz, E. Stocco, G. Trenins, B. Hirshberg, M. Rossi, and M. Ceriotti, I-PI 3.0: A flexible and efficient framework for advanced atomistic simulations, *The Journal of Chemical Physics* **161**, 062504 (2024).
- [48] G. Bussi, D. Donadio, and M. Parrinello, Canonical sampling through velocity rescaling, *Journal of Chemical Physics* **126**, 14101 (2007).
- [49] M. Ceriotti, G. Bussi, and M. Parrinello, Colored-noise thermostats à la Carte, *Journal of Chemical Theory and Computation* **6**, 1170 (2010).
- [50] J. Behler and M. Parrinello, Generalized Neural-Network Representation of High-Dimensional Potential-Energy Surfaces, *Physical Review Letters* **98**, 146401 (2007).
- [51] C. Malosso, F. Bigi, P. Pegolo, J. W. Abbott, P. Loche, M. Rossi, M. Ceriotti, and A. Mazitov, A high-quality, high-information dataset for universal atomistic machine learning, DOI: 10.24435/materialscloud:jc-9f (2026).
- [52] L. Talirz, S. Kumbhar, E. Passaro, A. V. Yakutovich, V. Granata, F. Gargiulo, M. Borelli, M. Uhrin, S. P. Huber, S. Zoupanos, C. S. Adorf, C. W. Andersen, O. Schütt, C. A. Pignedoli, D. Passerone, J. VandeVondele, T. C. Schulthess, B. Smit, G. Pizzi, and N. Marzari, Materials cloud, a platform for open computational science, *Scientific Data* **7**, 10.1038/s41597-020-00637-5 (2020).